

The effect of twist morphing on aerodynamic performance of finite wing at low Reynolds number

Yasemin B. Gunes¹, Ali Emirhan Eroğlu², Tahir Durhasan^{2*}, İlyas Karasu³, and Engin Pinar⁴

¹Adana Alparslan Türkeş Science and Technology University, Graduate School, Aerospace Engineering Department, 01250 Adana, Türkiye

²Adana Alparslan Türkeş Science and Technology University, Aeronautics and Astronautics Faculty, Aerospace Engineering Department, 01250 Adana, Türkiye

³Samsun University, Ozdemir Bayraktar Aeronautics and Astronautics Faculty, Aerospace Engineering Department, 55060 Samsun, Türkiye

⁴Cukurova University, Ceyhan Engineering Faculty, Mechanical Engineering Department, 01950 Adana, Türkiye

Abstract. This study experimentally investigates the effect of twist morphing on the aerodynamic characteristics of a finite wing at low Reynolds numbers (Re). As the base model, a NACA 0018 airfoil with an aspect ratio of 4 is used. The twist morphing configuration is obtained by applying camber deflection at the wing tip, while maintaining a symmetrical root section. Two morphing cases with trailing-edge deflection angles of $\theta = 2.5^\circ$ and 5° are examined at $Re = 7 \times 10^4$ and 10×10^4 . Force measurements and surface oil visualization experiments are carried out to depict the flow structure. The results show that twisted wings generate positive lift at an angle of attack of $\alpha = 0^\circ$. The lift coefficient (C_L) of the twisted morphing wings increases by up to 40% compared to the baseline case. Flow visualizations reveal that laminar separation bubbles (LSBs) occur at low angles of attack, and its size decreases with the increasing angle of attack. The interaction between tip vortices and LSBs further influences the local flow behaviour. The obtained results demonstrate that twist morphing can enhance aerodynamic efficiency and contribute to roll control in uncrewed aerial vehicles operating under low Reynolds number conditions.

1 Introduction

Morphing wing structures have attracted increasing research interest in recent years for their potential to improve aerodynamic performance in applications ranging from aerial vehicles to wind turbines. The shape-morphing can offer efficient solutions in response to varying flow regimes. In this context, various morphing strategies have been investigated in the literature, including the use of wing twist as a promising approach for aerodynamic performance. Introducing twist to the wing emphasizes its potential to improve aerodynamic efficiency and to optimize aerodynamics load distribution [1]. In particular, it contributes to flight control and the enhancement of flight performance in aerial vehicles.

The foundation of twist morphing research rooted in observations of biological systems [2]. Therefore, the deformation in the chordwise and spanwise directions during flight results in camber and twist morphing, respectively, which are commonly adopted from bio-inspired design principles [3]. In a recent review paper, Chen et al. [4] comprehensively investigated the flight dynamics and morphing structures of flying organisms, emphasized aerodynamic strategies in biological flyers by prioritizing biomimetic design principles. The

relation between flapping wing interaction and laminar separation bubbles (LSB) were specifically highlighted for low Reynolds number (Re) regimes. The implication potential from nature observations mostly focused on micro air vehicles (MAVs), specifically enhancing aerodynamic performance [5–7]. Rocchia et al. [8] developed a bio-inspired numerical simulation framework that combines an extended unsteady model with a general kinematic model capable of capturing complex wing deformations such as twisting and bending observed in insect and small bird flight. Their findings revealed that spanwise twisting and in-plane bending influence lift locally within the stroke cycle, whereas out-of-plane bending affects lift generation globally throughout the cycle, highlighting the important role of wing flexibility in enhancing aerodynamic performance at small scales. Guan and Yu [9] demonstrated that spanwise twist morphing in bat-inspired wings. Their results showed that twisting can increase the average lift by up to 25% and generate thrust instead of drag, revealing its functional similarity to the pitching motion observed in insect flight.

These insights have motivated the application of twist morphing concepts in micro air vehicle (MAV) designs, where controlled wing deformation is employed to mimic biological flight mechanisms and

* Corresponding author: tdurhasan@atu.edu.tr

achieve improved aerodynamic efficiency under varying flight conditions.

Furthermore, Kumkam et al. [10] numerically investigated the aeroelasticity of the various twisted wingtips to increase the structural stability during flight conditions of an uncrewed aerial vehicle (UAV) [11]. Runkel et al. [12] employed a twist angle of $\theta=2.5^\circ$ at the tips of their configurations, which have a thickness of 0.15 mm and a fibre structure of 20° , capable of creating twist deformation in aerodynamic load effectiveness. Their main was to investigate the structural behavior. Along with this, the lift coefficient C_L decreased by 10% and the wing root bending moment decreased by 22%.

Moreover, researchers continue to conduct studies in order to develop the wings with high aerodynamic efficiency by experimenting with different twist configurations. Rodrigue et al. [13] designed a twist-morphing segment capable of achieving up to 6.25° of twist at the wing tip to examine the aerodynamic performance at low angles of attack. In wind tunnel tests conducted at a flow velocity of 15 m/s, a 13% improvement in the lift-to-drag (C_L/C_D) ratio was achieved at an angle of attack of $\alpha = 2^\circ$. For $\alpha \leq 6^\circ$, the lift coefficient (C_L) showed significant increases, whereas the drag coefficient (C_D) exhibited only a limited rise. These results demonstrate that twist morphing can provide notable aerodynamic benefits over baseline wing configurations at low angles of attack. Also, for wind turbine blades, twist morphing structures have been demonstrated to passively manipulate flow physics and enhance system performance [14–16].

In addition to twist morphing, a membrane wing was also employed to enhance the aerodynamic efficiency, as morphing wings generally provide an improved lift coefficient (C_L), albeit with an increase in drag coefficient (C_D), compared to the baseline configurations [17,18]. Furthermore, in a separate study, the effects of vortex structures formed on micro air vehicle wings on lift performance were examined. The results showed that the twisted wing generated approximately 65% higher lift coefficient (C_L) compared to the non-twisted configuration [19]. Furthermore, applying a flexible surface to the suction side of an airfoil can delay stall and increase the stall angle for finite wings [20].

The aerodynamic benefits of controlled spanwise deformation have been shown in previous studies, specifying wing flexibility and spanwise twisting role in small scales. However, the aerodynamic effects of twist morphing on finite wing geometries have not yet been thoroughly investigated. The present study aims to examine the influence of twist morphing as an aerodynamic control strategy under low Reynolds number flow regimes and to assess its implications for flight control. For this purpose, experimental investigations are conducted on a NACA0018 airfoil with twist formations applied at the spanwise tip for twist angles of $\theta = 2.5^\circ$ and 5° at Reynolds number, $Re = 7 \times 10^4$ and 10×10^4 . Aerodynamic coefficients and oil surface visualizations for the twist morphing cases are presented and compared with the baseline configuration.

The findings are expected to provide a foundation for enhancing aerodynamic performance in uncrewed aerial vehicles (UAVs) and small-scale wind turbines.

2 Material and method

The experimental investigations were performed in a low-speed, suction-type wind tunnel located in the Aerodynamics Laboratory of the Department of Aerospace Engineering at Adana Alparslan Türkeş Science and Technology University. The tunnel features a square test section measuring $600\text{mm} \times 600\text{mm}$, enclosed by transparent plexiglass walls to enable clear visualization of the flow field. The facility can operate at airspeeds up to 20 m/s, with a turbulence intensity below 1 % under the present test conditions in which satisfies the low-speed wind tunnel test conditions [21]. A schematic representation of the experimental arrangement is provided in Figure 1, illustrating the airfoil model equipped with a servo motor for angle-of-attack adjustment and a six-component load cell used for aerodynamic force measurements.

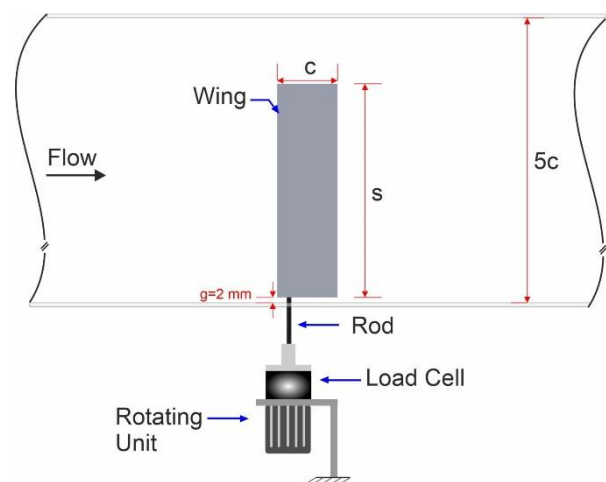


Fig. 1. Experimental set up.

The chord (c) and spanwise (s) lengths of the NACA0018 airfoil are $c = 120$ mm and $s = 480$ mm, respectively. Figure 2 presents the schematic twist morphing concept. The airfoil is shown in spanwise projection with the root section fixed and the tip section deflected (i.e., cambered) about the local chord axis. The camber deflection on the tip section is obtained using the FishBAC concept utilized by Wood et al. [22]. In the present study, the deflection starts at the chordwise location of $x/c=0.35$, and the morphed part of the airfoil is defined by a third-order polynomial function. Also, the inset highlights the normalized airfoil coordinates of a NACA 0018; the black trace is the base mode (no twist) airfoil, the blue traces denote the deformed tip airfoils, resulting the red line as the indication of local chord rotation used to define the twist angle θ . This morphing concept enables easy implementation in UAVs by maintaining the leading edge fixed while deflecting the wing profile. In addition to the base model ($\theta=0^\circ$), two twist morphing cases ($\theta=2.5^\circ$ and 5°) were created to perform this study. Based on the chord lengths, two low Reynolds numbers

were investigated throughout the study ($Re=7 \times 10^4$ and 10×10^4).

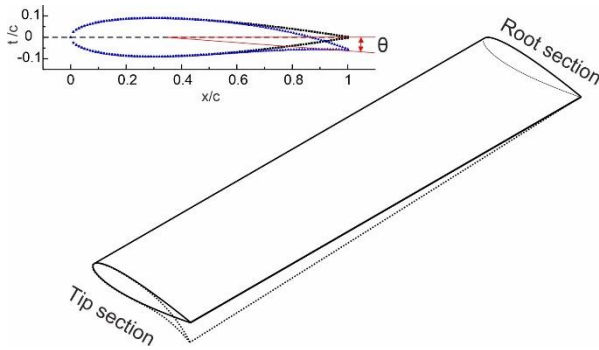


Fig. 2. Spanwise twist morphing of the airfoil.

Aerodynamic force coefficients were calculated using Equations 1 and 2.

$$C_L = \frac{F_L}{0.5\rho U_\infty A} \quad (1)$$

$$C_D = \frac{F_D}{0.5\rho U_\infty A} \quad (2)$$

where ρ , U_∞ and A present the density of air, free-stream velocity, and reference area of the airfoil, respectively. The measurement uncertainty in the evaluated force coefficients was determined to be less than 3%, remaining well within the acceptable range reported in previous studies [23,24].

Surface oil flow visualization was performed to examine the influence of laminar separation bubble (LSB) and tip vortex on the flow pattern over the upper surface (i.e., suction surface) of the wing at angles of attack $\alpha=4^\circ, 8^\circ$, and 12° . The matte black airfoil surfaces were coated with the oil mixture and allowing the airflow to dry it. The oil mixture was prepared using kerosene, titanium dioxide, and a trace amount of oleic acid. This mixing method was also employed in our previous study [20].

3 Results and discussion

Figures 3, 4, and 5 present the aerodynamic coefficients distribution of base NACA 0018 ($\theta=0^\circ$) and two twisted morphing wings with respect to various angles of attack $0^\circ \leq \alpha \leq 18^\circ$ for Reynolds numbers of $Re=7 \times 10^4$ and $Re=10 \times 10^4$.

The lift coefficient (C_L) variation in Figure 3 reveals significant performance enhancement through twisted morphing cases. At both Reynolds numbers, the twisted configurations demonstrate notable lift generation throughout pre-stall regime. At $\alpha=0^\circ$, twisted cases produce lift in increasing trend with the increase of Re number. With the increase of twist angle from $\theta=2.5^\circ$ to $\theta=5^\circ$, it achieves approximately 40% higher C_L values compared to base model at low angles of attack ($\alpha \leq 8^\circ$). Moreover, the reason of why $\theta=5^\circ$ yielding better results would give us to understand spanwise redistribution of the effective angle of attack, which optimizes the local loading distribution and delays the onset of flow separation. Maximum lift coefficients occur at approximately 9° and 10° for all configurations. With

the increase of Re number, the stall is delayed specifically for $\theta=2.5^\circ$ twisted case. For post stall conditions ($\alpha \geq 12^\circ$), it is observed that C_L distribution is having relatively uniform degradation among all configurations, while the twisted cases maintain a slight performance advantage even in the fully separated regime.

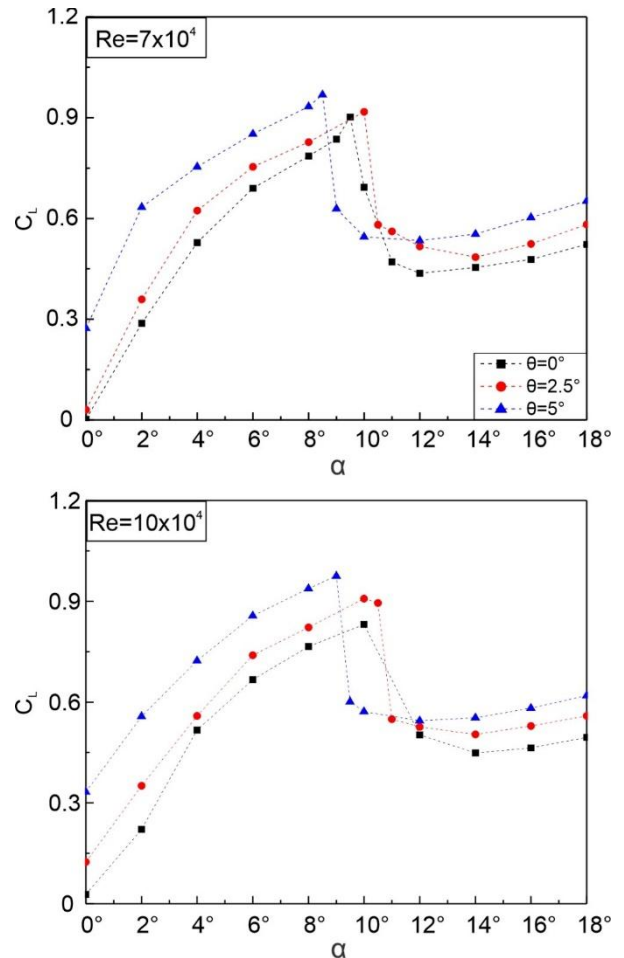


Fig. 3. Lift coefficients with respect to angle of attack.

Figure 4 reveals the drag coefficient (C_D) profiles, and it demonstrates the aerodynamic penalty associated with the twist morphing, particularly at higher angles of attack. With the increase of twist angle, the wing generates more drag force on the body for all Re numbers. For $\theta=2.5^\circ$ twisted case, C_D values exhibit relative similar drag trends in comparison with the base case ($\theta=0^\circ$). However, a critical jump of C_D occurs at the onset of stall. Also, the $\theta=5^\circ$ twisted configuration consistently produces the higher drag compared to the other cases. With the increase of Re number, it is obtained that slightly higher C_D values specifically for $\theta=5^\circ$ case in the mid-angles of attack range ($\alpha = 8^\circ - 12^\circ$). The post-stall ($\alpha > 12^\circ$) regime reveals monotonically increasing drag for all cases. This drag penalty would be the primary trade-off for the enhanced lift performance observed at lower angles of attack.

Figure 5 provides the lift to drag ratio (C_L/C_D) distributions to evaluate the aerodynamic performance. Since the base model benefits from both adequate lift generation and minimal drag for $Re=7 \times 10^4$, this configuration achieves the highest peak of C_L/C_D value

at $\alpha=6^\circ$. Also, for $Re=7 \times 10^4$, it can be observed a threshold at $\alpha=4^\circ$, indicating a transition region of C_L/C_D ratio. With the increase of $Re=10 \times 10^4$, the ratios C_L/C_D are higher for the twisted morphing cases at $\alpha \leq 4^\circ$. At very low angles of attack, the $\theta=5^\circ$ twisted wing demonstrates superior C_L/C_D ratios due to substantially higher lift coefficients that outweigh the modest drag increase. The C_L/C_D curves exhibit distinct maxima, with the baseline peaking at $\alpha=6^\circ$, while twisted configurations achieve maximum efficiency at slightly lower angles. This shift suggests that twisted models operate optimally at reduced angles of attack where their enhanced lift capability provides maximum benefit without incurring excessive drag penalties. For the post-stall regime, the degradation of C_L/C_D ratios is precipitous for all configurations. In this regime, all configurations exhibit similar poor efficiency, indicating that blade twist provides no advantage in fully separated flow conditions.

Overall, a critical finding is that while twisted configurations enhance lift generation substantially, this does not universally translate to improved aerodynamic efficiency. The $\theta=5^\circ$ twist configuration, despite producing the highest lift coefficients, exhibits the lowest peak C_L/C_D due to its elevated drag profile. This indicates that the optimal twist angle involves a compromise between lift enhancement and drag minimization. The $\theta=2.5^\circ$ twisted model emerges as a potential compromise solution, offering lift improvements over the baseline while maintaining peak C_L/C_D values close enough to base model.

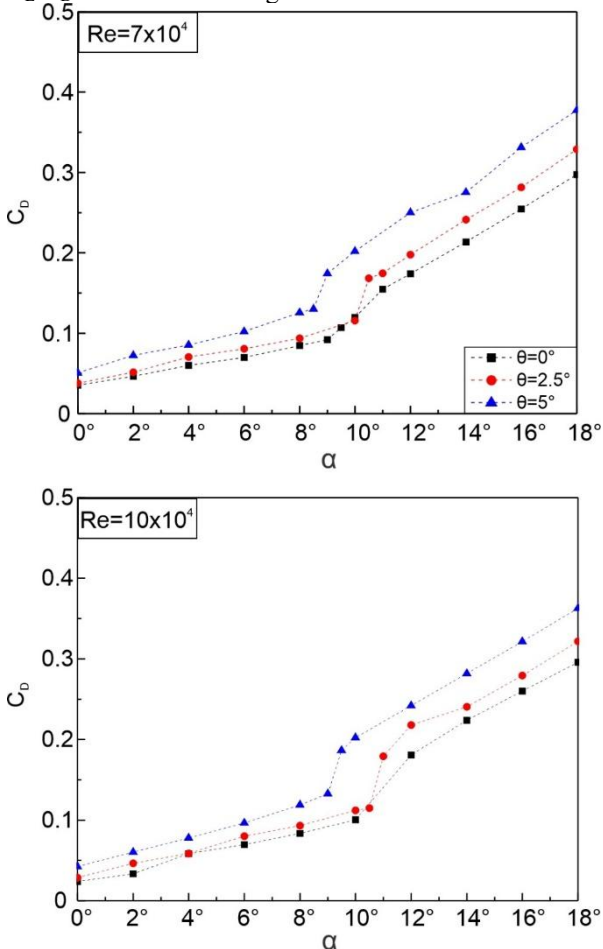


Fig. 4. Drag coefficients with respect to angle of attack.

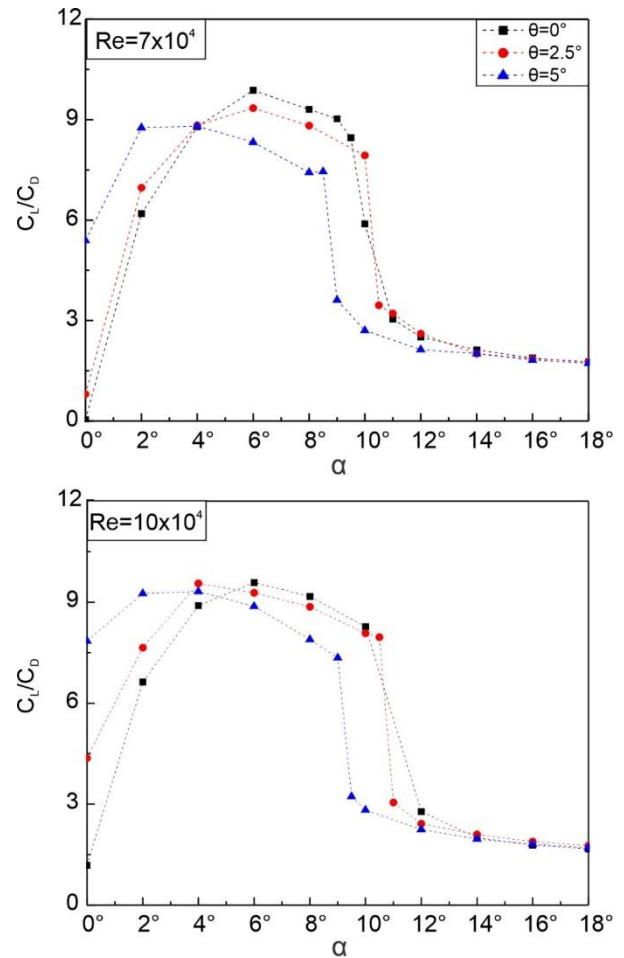


Fig. 5. Lift-to-drag coefficients with respect to angle of attack.

Figures 6, 7, and 8 reveal the surface oil flow visualization results at $Re=10 \times 10^4$ for $\alpha=4^\circ$, 8° , and 12° , respectively. At $\alpha=4^\circ$, the laminar separation bubble (LSB) occurs at chordwise location between $0.2 \leq x/c \leq 0.5$, while the formation of tip vortex causes chaotic flow patterns (designated with the blue line in these figures) for $\theta=0^\circ$. The mutual interaction between the tip vortex system (V_T) and these LSBs plays a decisive role in shaping the local flow characteristics and spanwise aerodynamic loading. The size of LSBs slightly changes for $\theta=2.5^\circ$ in comparison with the $\theta=0^\circ$ model. However, it significantly increases when the twist angle raised from $\theta=2.5^\circ$ to 5° due to early separation of the boundary layer. The LSBs on the wing are observed between $0.1 \leq x/c \leq 0.5$ for the $\theta=5^\circ$ model. The separation and reattachment points move closer to the leading edge of the wing with the increasing angles of attack. The LSBs remarkably shrinks and are located approximately at $0.1 \leq x/c \leq 0.3$ when the angle of attack reaches $\alpha=8^\circ$ for all models. The visualizations obtained at $\alpha=12^\circ$ indicate the post-stall condition where separated boundary layer from the leading edge is not reattached the surface. Therefore, aerodynamic efficiency of wings deteriorates. The tip vortices are present in all models.

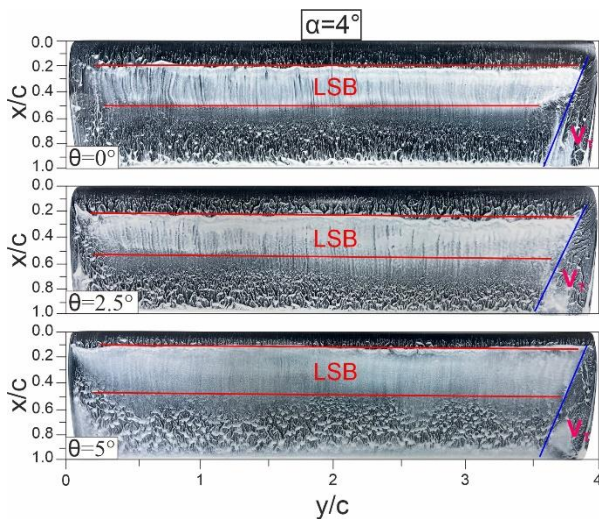


Fig. 6. Surface oil visualization at $\alpha = 4^\circ$.

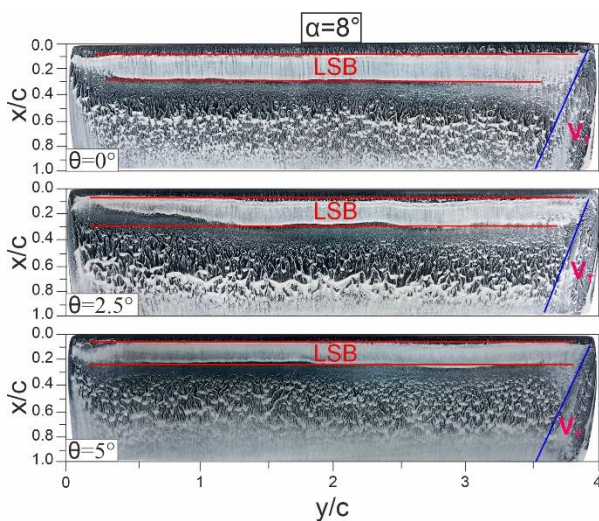


Fig. 7. Surface oil visualization at $\alpha = 8^\circ$.

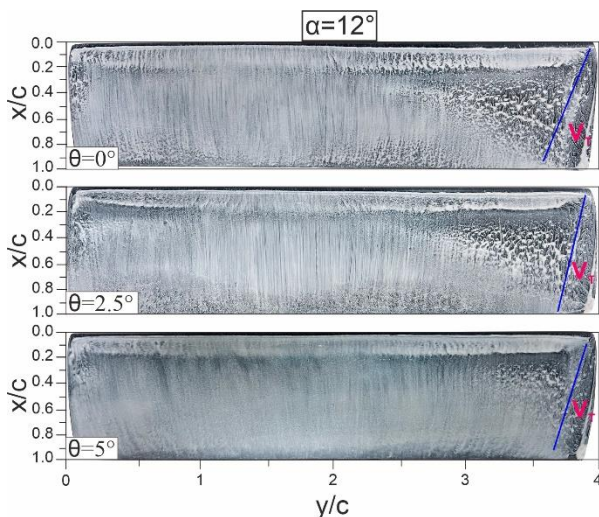


Fig. 8. Surface oil visualization at $\alpha = 12^\circ$.

4 Conclusion

This experimental investigation has systematically examined the aerodynamic performance of twist morphing of a NACA 0018 finite wings through wind tunnel testing at low Reynolds numbers. The study demonstrates that twist morphing, achieved through

trailing-edge deflection at the wing tip ($\theta = 2.5^\circ$ and 5°), significantly alters the aerodynamic characteristics and flow topology of the wing operating at $Re = 7 \times 10^4$ and 10×10^4 .

The force measurement results confirm that twist morphing provides substantial lift enhancement especially for at low angle of attacks ($\alpha \leq 8^\circ$). The $\theta = 5^\circ$ deflection case achieving up to 17% increase in maximum lift coefficient compared to the baseline untwisted configuration (base case, $\theta = 0^\circ$). A notable feature of the twisted wings is their ability to generate positive lift at zero angle of attack. The $\theta = 2.5^\circ$ twist configuration emerges as an optimal compromise, offering improvements in maximum lift approximately 8% while maintaining aerodynamic efficiency comparable to the base model.

However, the enhanced lift generation comes with an increased drag. The $\theta = 5^\circ$ twisted configuration exhibits drag coefficients two times higher than the baseline at angles of attack exceeding $\alpha = 10^\circ$, resulting in reduced peak lift-to-drag ratios. Despite this drag penalty, the aerodynamic efficiency analysis reveals that twisted configurations outperform the baseline at low angles of attack, where the substantial lift gains outweigh the modest drag increases. This identifies an optimal operational envelope for twist-morphed wings between $\alpha = 2^\circ - 8^\circ$, where aerodynamic benefits are maximized.

Surface oil flow visualization at $Re = 10 \times 10^4$ provides critical insights into the underlying flow physics. The visualizations reveal the presence of laminar separation bubbles (LSBs) on the wing surface at low angles of attack, which progressively diminish in size as angle of attack increases. The complex interaction between wing tip vortices and these LSBs fundamentally influences the local flow behavior and spanwise load distribution.

In conclusion, twist morphing represents a promising aerodynamic control strategy for low Reynolds number applications, offering substantial lift enhancements within a defined operational envelope. The optimal twist angle depends on the specific mission requirements: higher twist angles ($\theta = 5^\circ$) maximize lift generation for takeoff and maneuvering, while moderate twist angles ($\theta = 2.5^\circ$) provide a balanced trade-off between lift enhancement and aerodynamic efficiency for cruise flight.

The authors sincerely acknowledge the financial support provided by the Scientific and Technological Research Council of Türkiye (TUBITAK) through Grant Number 223M340.

References

1. S. Heathcote, Z. Wang, and I. Gursul, *J. Fluids Struct.* **24**, 183 (2008)
2. C. Harvey, L. L. Gamble, C. R. Bolander, D. F. Hunsaker, J. J. Joo, and D. J. Inman, *Prog. Aerosp. Sci.* **132**, 100825 (2022)
3. A. K. Stowers and D. Lentink, *Bioinspir. Biomim.* **10**, 025001 (2015)

4. D. Chen, L. Fu, C. Hefler, T. Ji, R. Noda, M. Pittman, H. Qiu, W. Shyy, and Q. Zhang, *Acta Mech. Sin.* **41**, 325312 (2025)
5. L. Zheng, T. L. Hedrick, and R. Mittal, *PLOS ONE* **8**, e53060 (2013)
6. H.-V. Phan and D. Floreano, *Sci. Robot.* **9**, eado3890 (2024)
7. T. Nakata, R. Noda, and H. Liu, *J. Biomech. Sci. Eng.* **13**, 17 (2018)
8. B. A. Rocca, S. Preidikman, M. L. Verstraete, and D. T. Mook, *J. Aerosp. Eng.* **30**, 04016079 (2017)
9. Z. Guan and Y. Yu, *Appl. Math. Mech.* **35**, 1607 (2014)
10. N. Kumkam, N. Suratemeekul, and S. Slesongsom, *Biomimetics* **10**, (2025)
11. P. Bagul, Z. A. Rana, K. W. Jenkins, and L. Könözsy, *Chin. J. Aeronaut.* **33**, 1154 (2020)
12. F. Runkel, U. Fasel, G. Molinari, A. F. Arrieta, and P. Ermanni, *Compos. Struct.* **206**, 750 (2018)
13. H. Rodrigue, S. Cho, M.-W. Han, B. Bhandari, J.-E. Shim, and S.-H. Ahn, *J. Mech. Sci. Technol.* **30**, 229 (2016)
14. S. Thel, D. Hahn, M. Haupt, and S. Heimbs, *Struct. Multidiscip. Optim.* **65**, 155 (2022)
15. P. L. Bishay, T. McKinney, G. Kline, M. Manzo, A. Parian, D. Bakhshi, A. Langwald, A. Ortega, M. Gagnon, and G. Funes Alfaro, *J. Eng. Res.* **12**, 931 (2024)
16. M. S. Genç, H. H. Açikel, and K. Koca, *Energy Convers. Manag.* **219**, 113042 (2020)
17. N. I. Ismail, A. H. Zulkifli, M. Z. Abdullah, M. Hisyam Basri, and N. Shah Abdullah, *Chin. J. Aeronaut.* **26**, 1093 (2013)
18. N. I. Ismail, A. H. Zulkifli, M. Z. Abdullah, M. H. Basri, and N. S. Abdullah, *Chin. J. Aeronaut.* **27**, 475 (2014)
19. N. Ismail, A. Zulkifli, R. Talib, H. Yusoff, and M. A. Tasin, *Int. J. Micro Air Veh.* **8**, 194 (2016)
20. A. E. Eroğlu, T. Durhasan, J. R. Jafari, and İ. Karasu, *Çukurova Üniversitesi Mühendis. Fakültesi Derg.* **40**, 61 (2025)
21. J. B. Barlow, W. H. Rae, and A. Pope, *Low-Speed Wind Tunnel Testing* (John Wiley & Sons, 1999)
22. B.K. Woods, J.H. Fincham, and M.I. Friswell, Aerodynamic modelling of the fish bone active camber morphing concept, In Proceeding of the the RAeS Applied Aerodynamics Conference, Bristol, UK, 22-24 July (2014)
23. M. S. Genç, İ. Karasu, and H. Hakan Açikel, *Exp. Therm. Fluid Sci.* **39**, 252 (2012)
24. M. M. Aksoy, *Ocean Eng.* **341**, 122584 (2025)